Journal of Solid State Chemistry **161,** 179–183 (2001)
doi:10.1006/jssc.2001.9247, available online at http://www.idealibrary.com on IDEAL®

Synthesis and Characterization of Ternary $CuInS_2$ Nanorods via a Hydrothermal Route

Jianping Xiao, Yi Xie,[1] Rui Tang, and Yitai Qian

Structure Research Laboratory, and Laboratory of Nanochemistry & Nanomaterials, University of Science and Technology of China, Hefei, Anhui 230026, People's Republic of China

Received February 27, 2001; in revised form April 26, 2001; accepted May 11, 2001; published online July 16, 2001

Well-defined ternary $CuInS_2$ nanorods 20–25 nm in diameter and 400–450 nm in length were synthesized by the reaction of $CuCl_2$, In, CS_2, and NaOH at temperature as low as 180°C for 15 h when water was used as the solvent. The products were characterized by X-ray diffraction, transmission electron microscopy, selected area electron diffraction, X-ray photoelectron spectroscopy, and UV–vis absorption spectroscopy techniques. Experimental results indicate that reaction temperature is an important factor in this approach and liquid indium plays an important role in the formation of $CuInS_2$ nanorods. Finally, a solution–liquid–solid mechanism was proposed for the nanorod growth. © 2001 Academic Press

Key Words: **$CuInS_2$ nanorods; hydrothermal route; CS_2; liquid indium.**

1. INTRODUCTION

The large interest in nanostructures results from their numerous potential applications in various areas such as materials and biomedical sciences, electronics, optics, magnetism, energy storage, and electrochemistry (1). Nanostructural materials can often display optical, electronic, and structural properties different from those of their bulk counterparts (2,3). Currently, one-dimensional nanoscale materials have attracted much attention due to their interesting physical properties and potential device applications (4). Therefore, the synthesis of nanowires, nanorods, or nanofibers and the investigation of their properties have aroused considerable interest (2). The control of nucleation and growth of one-dimensional nanostructural material is becoming critical. The study of nucleation and growth mechanisms will help us to understand and control these processes at the atomic level via the synthetic chemistry employed.

Due to its direct energy gap of 1.5 eV, ternary compound $CuInS_2$ with the chalcopyrite structure, which belongs to the I–III–VI_2 family, has emerged as a leading material for high-efficiency and radiation-hard solar cell applications (5). In addition, $CuInS_2$ is a candidate for the cathode material of photochemical devices owing to its high performance and high output stability (6). $CuInS_2$ can be synthesized by a variety of methods such as solid-state reaction at elevated temperature (7), electrodeposition (8), spray pyrolysis (9), sputtering (10), multi- and single source chemical vapor deposition (CVD) (11), and ionized cluster beam technique (12). However, these methods require either very high temperature (typically 600–900°C), high pressure, or special apparatus. In addition, these methods are of relatively long reaction time and it is difficult to get satisfactory stoichiometry. Recently, Parkin and co-workers obtained $CuInS_2$ by refluxing a mixture of $CuCl_2$, $InCl_3$, and Na_2S in toluene for 72 h, but posttreatment at 500°C for 24 h was necessary to get crystals (13).

It is well known that the device properties of $CuInS_2$-based solar cells are badly affected by their stoichiometeric composition, defect, and structure, which are strongly related to preparation conditions. For example, the density of stacking faults and dislocation lines on the [112] crystal plane is much higher for the Cu-poor $CuInS_2$ film compared with the Cu-rich $CuInS_2$ film, which leads to a difference in the conversion efficiency of the optoelectronic device (14). Recently, various solution chemical synthesis techniques have been utilized to prepare some fascinating materials. This chemical method allows the particle size and their distribution as well as their morphology to be controlled (15). In our group, Lu *et al.* synthesized irregular $CuInS_2$ nanoparticles at 200°C through a solvothermal process using CuCl, In, and S as reagents; however, they could not control the products to grow nanorods (16). Jiang *et al.* prepared $CuInS_2$ nanorods at 280°C for 48 h through elemental solvothermal reaction (17).

[1]To whom correspondence should be addressed.

0022-4596/01 $35.00

Very recently, a solution–liquid–solid (SLS) mechanism was developed to grow well-crystallized semiconductor fibres at greatly decreased temperatures (18). The SLS is closely analogous to the well-known vapor–liquid–solid (VLS) mechanism (19), in which whisker crystals grow from flux droplets that are fed from the vapor phase rather than a solution phase. In this paper, we report a hydrothermal pathway to ternary $CuInS_2$ nanorods with $CuCl_2 \cdot 2H_2O$, In, CS_2, and NaOH as reagents at 180°C. The synthetic reaction was carried out in an autoclave and can be represented by Eq. [1]:

$$3CuCl_2 \cdot 2H_2O + CS_2 + In + 6NaOH \xrightarrow{H_2O}$$

$$CuInS_2 + Na_2CO_3 + 4NaCl + 2CuCl + 9H_2O. \quad [1]$$

In this process, carbon disulfide was used as the sulfur source and NaOH as the attacking reagent to release S^{2-} (20).

2. EXPERIMENTAL

All reagents were of analytical grade and were used without further purification. In a typical procedure, the product $CuInS_2$ can be synthesized from a stoichiometric mixture of $CuCl_2 \cdot 2H_2O$ (1.023 g, 6 mmol), In (0.23 g, 2 mmol), CS_2 (0.152 g, 2 mmol), and NaOH (0.48 g, 12 mmol). The reactants were added into a 50-mL Teflon-lined autoclave, which was then filled with distilled water up to 85% of the total volume. The autoclave was sealed and maintained at 180°C for 15 h, and then allowed to cool to room temperature naturally. The precipitate was filtered off, washed with dilute HNO_3, aqueous ammonia solution, absolute ethanol and distilled water in sequence, and then dried under a vacuum at 50°C for 4 h. The product was collected for characterization. In order to investigate the reaction mechanism, this reaction was also performed at 150°C (below the melting point of In).

The obtained product was characterized by X-ray powder diffraction (XRD) using a Japan Rigaku D/max-rA X-ray diffractometer with graphite-monochromatized Cu$K\alpha$ radiation ($\lambda = 1.54178$ Å). The scan rate of $0.05^\circ\ s^{-1}$ was applied to record the patterns in the 2θ range of 10–70°. Transmission electron microscopy (TEM) image and selected area electron diffraction (SAED) pattern were obtained on a Hitachi Model H-800 with an accelerating voltage of 200 kV. In order to derive the composition information about the product, X-ray photoelectron spectroscopy (XPS) was performed on an ESCALab MKII X-ray photoelectron spectrometer, using Mg$K\alpha$ X ray as the excitation source. UV–vis absorption spectroscopy was performed on a JGNA Specord 200 PC UV–vis spectrophotometer when ethanol was used as a reference.

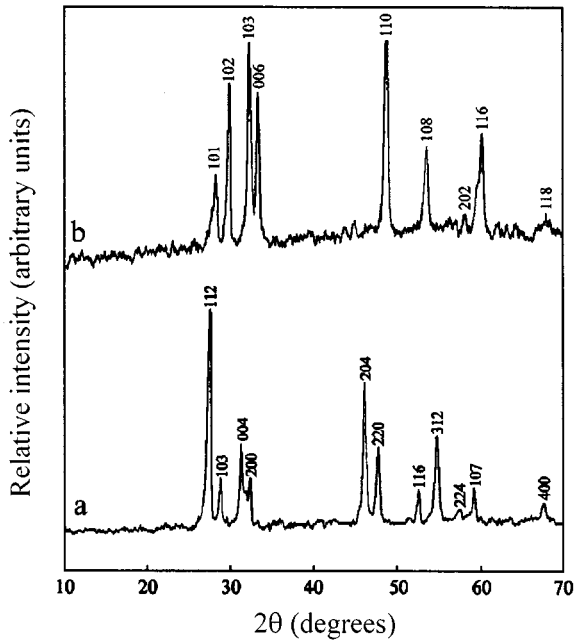

FIG. 1. XRD patterns of the products obtained by the hydrothermal pathway at different temperatures: (a) tetragonal $CuInS_2$ prepared at 180°C and (b) hexagonal CuS prepared at 150°C.

3. RESULTS AND DISCUSSION

The XRD pattern of a typical sample prepared at 180°C is shown in Fig. 1a, indicating only the chalcopyrite phase with an intense peak at $2\theta = 27.8^\circ$ oriented along the [112] crystal plane. All the diffraction peaks can be indexed to tetragonal $CuInS_2$ with cell constants $a = 5.514$ Å and $c = 11.139$ Å, which is in agreement with the reported data in the literature ($a = 5.523$ Å and $c = 11.141$ Å) (21). However, a relatively strong [004] peak in the pattern indicates a weakly preferential orientation of [001] in $CuInS_2$ nanorods. No characteristic peaks of other impurities such as In or copper sulfides were observed. According to the Scherrer formula (22) based on the half-width of XRD peaks, the average crystalline size of the nanorods is estimated as 22.1 nm. Figure 1b shows the XRD pattern of the sample prepared at 150°C, showing that the as-prepared product can be indexed to hexagonal CuS (JCPDS No. 6-464). This results clearly indicates that the reaction temperature is an important factor in this approach. When the reaction temperature is lower than the melting point of In, this reaction proceeds to produce CuS and cannot continue to form $CuInS_2$ because of the low reactivity of In.

TEM image for the sample prepared at 180°C is shown in Fig. 2a, indicating that the as-obtained products are well-defined nanorods with diameters of 20–25 nm and lengths ranging from 400 to 450 nm. The SAED pattern (Fig. 2b) is

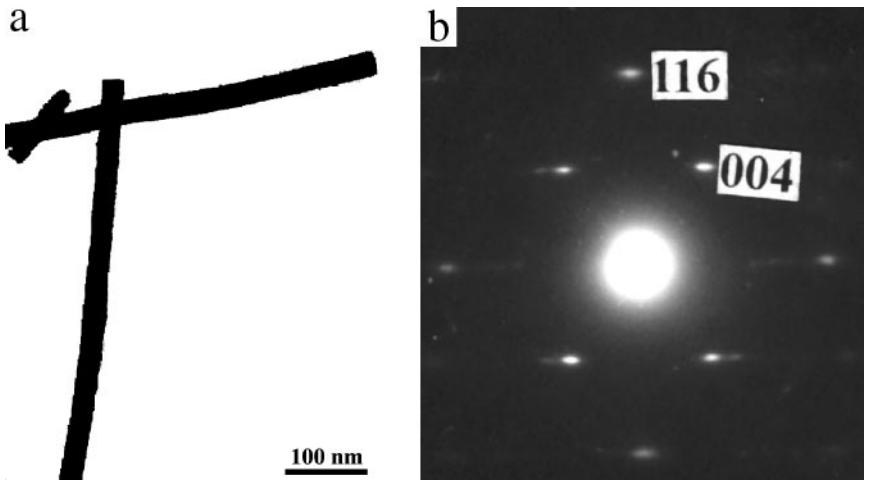

FIG. 2. (a) TEM image of $CuInS_2$ nanorods and (b) SAED pattern of $CuInS_2$ nanorods.

consistent with the single-crystalline nature of the nanorods. These diffraction dots can be divided into two series: one is caused by the [004] crystal plane; the other is caused by the [116] plane.

The XPS technique was carried out to obtain composition information about the sample prepared at 180°C. A survey spectrum is shown in Fig. 3a, indicating the presence of Cu, In, and S as well as C from reference and O impurity. Oxygen in the sample is likely due to exposure to the atmosphere since nanocrystalline material exhibits a high surface area-to-volume ratio. There are no peaks for Cl or Na from the reactants and other peaks, indicating that the as-obtained product is relatively pure.

High-resolution spectra were also taken for the Cu 2*p* region, the In 3*d* region, and the S 2*p* region in order to determine the valency state and atomic ratio. The Cu 2*p* core level spectrum is shown in Fig. 3b, indicating that the observed values of the binding energies for Cu $2p_{3/2}$ and Cu $2p_{1/2}$ are consistent with the literature values (23). The full width at half-maximum for Cu $2p_{3/2}$ and Cu $2p_{1/2}$ peaks are 1.9 and 2.3 eV, respectively, which are also in good agreement with the literature values for Cu^+ (24). In addition, the Cu $2p_{3/2}$ satellite peak of Cu^{2+}, which is usually centered at 942 eV (25), does not appear in the spectrum. Therefore, it can be concluded that only Cu^+ exists in the sample, indicating that Cu^{2+} of the starting material was reduced during the course of reaction. Figure 3c is the typical In 3*d* core level spectrum, showing that the strong peak at 444.8 eV corresponds to the In $3d_{5/2}$ binding energy for $CuInS_2$ (23). The In $3d_{5/2}$ binding energy of elemental In is usually located at 443.8 eV (23), indicating that elemental In was oxidized during the hydrothermal treatment. The S 2*p* core level spectrum (Fig. 3d) shows two peaks (namely the presence of two chemical environment): one at 161.2 eV corresponding to S from Cu–S and the other at 162.4 eV corresponding to S from In–S (23). For three core level spectra, there was no evidence of shake-up peaks, which are photoemission peaks from species ionized prior to the observed photoemission process and generally occur several electronvolts higher than the binding energy of the main peaks in the spectra. The quantification of the peaks gives a Cu : In : S ratio of 0.96 : 1 : 2.04, which is close to the stoichiometry of $CuInS_2$.

In this process, $CuCl_2$, CS_2, and In play important roles in the formation of $CuInS_2$ nanorods. CS_2 can be attacked by NaOH to release S^{2-}, which can make this reaction proceed at relatively low temperatures. When CS_2 was replaced by S powder with other reaction conditions kept constant, many diffraction peaks appeared in the XRD pattern, which could be indexed to copper sulfides and unreacted In, but no characteristic peaks of tetragonal $CuInS_2$ appeared. $CuCl_2$, as an oxidizing reagent, can oxidize elemental In to In^{3+} ($\varphi^{\theta}_{Cu^{2+}/CuCl} = 0.538$ V, $\varphi^{\theta}_{Cu^{2+}/Cu^{+}} = 0.538$ V, $\varphi^{\theta}_{In^{2+}/In} = -0.343$ V) under proper reaction conditions, which is also important for the formation of the product. When $CuCl_2$ was displaced by CuCl, there was no formation of $CuInS_2$. In this electron-transfer reaction, liquid In also plays an important role in the formation of $CuInS_2$ nanorods when the reaction temperature is higher than the melting point of In (157°C). At the reaction temperature, S^{2-} can react with In^{3+} to form $(InS_2)^-$ dissolved in liquid In. Cu^+ ion then reacts at the growth site with $(InS_2)^-$ to form the product. The following reactions may occur:

$$CS_2 + 6NaOH \rightarrow 2Na_2S + Na_2CO_3 + 3H_2O \qquad [2]$$

$$3CuCl_2 + In \rightarrow 3CuCl + InCl_3 \qquad [3]$$

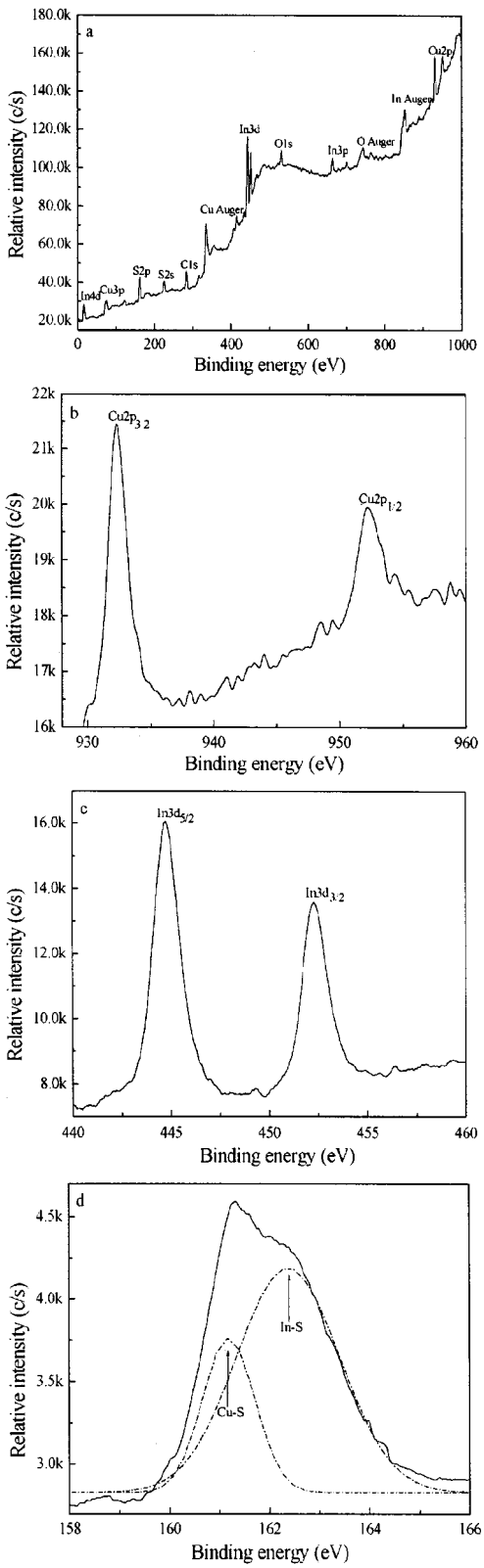

FIG. 3. XPS spectra of $CuInS_2$ nanorods: (a) typical XPS survey spectrum of $CuInS_2$ nanorods, (b) core level spectrum for Cu 2*p*, (c) core level spectrum for In 3*d*, and (d) core level spectrum for S 2*p*.

$$2S^{2-} + In^{3+} \rightarrow (InS_2)^- \quad [4]$$

$$CuCl \Leftrightarrow Cu^+ + Cl^- \quad [5]$$

$$Cu^+ + (InS_2)^- \rightarrow CuInS_2. \quad [6]$$

The existence of liquid In may motivate this electron-transfer reaction to grow $CuInS_2$ nanorods. This mechanism resembles that of the complex solution–liquid–solid (SLS) proposed for the growth of InP nanofibers by Buhro's research group (18). At the synthetic temperature (above the melting point of In), the metal particle would melt (liquid state) and provide an energetically favored site for the absorption of solution-phase reactants (solution state), which benefits the growth of nanorods (solid state) significantly. Since the SLS mechanism cannot function without liquid In, the reaction at temperatures below the melting point of In should not produce rods or fibers. The failure to obtain rods at 150°C further confirmed the proposed mechanism.

The structural property of $CuInS_2$ nanorods is also reflected in the absorption spectrum (Fig. 4). A minor absorption shoulder peak at about 825 nm is observed, which can be regarded as the optical transition of the first excitonic state and is in agreement with that of the bulk $CuInS_2$ (827 nm). The result indicates that as-obtained $CuInS_2$ nanorods are too large for quantum confinement, and in fact the Bohr exciton radius for $CuInS_2$ is 3.2 nm, which can be calculated according to Refs. (26,27). The average particle diameter, as calculated from the maximum of the absorption curve ($\lambda_m = 825$ nm), is 21 nm (28), which is consistent with the TEM and XRD results. Since the onset of the absorption spectrum generally represents the larger end of the size distribution (29), the position of the absorption edge ($\lambda_e = 1000$ nm) shows the length of the nanorods (400–450 nm). The large difference between sizes calculated

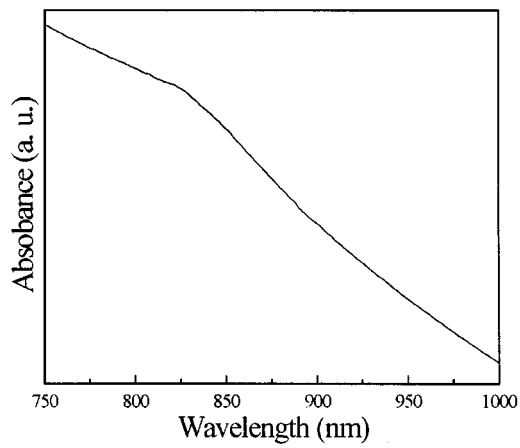

FIG. 4. UV–vis absorption spectrum of $CuInS_2$ nanorods dispersed in ethanol.

from λ_e and λ_m, which may be related to the width of particle size distribution, is characteristic of nanorods.

4. CONCLUSION

In summary, $CuInS_2$ nanorods with diameters of 20–25 nm and lengths of 400–450 nm have been synthesized via a hydrothermal pathway at 180°C for 15 h. TEM images confirmed the morphology of the as-obtained products. Experimental results indicate that the reaction temperature is an important factor in this approach and liquid indium plays an important role in the formation of $CuInS_2$ nanorods. The SLS mechanism is likely responsible for the nanorod growth.

ACKNOWLEDGMENTS

Financial support from the Chinese National Science Foundation of Natural Science Research and the Chinese Ministry of Education is gratefully acknowledged.

REFERENCES

1. A. Huczko, *Appl. Phys. A Mater. Sci. Processing* **70,** 365 (2000).
2. A. P. Alivisatos, *Science* **271,** 933 (1996).
3. L. E. Brus, *J. Chem. Phys.* **80,** 4403 (1984).
4. J. Hu, T. W. Odom, and C. M. Lieber, *Acc. Chem. Res.* **32,** 435 (1999).
5. R. W. Birkmire and E. Eser, *Annu. Rev. Mater. Sci.* **27,** 625 (1997).
6. D. Cahen, G. Dagan, Y. Mirovsky, G. Hodes, W. Giriat, and M. Lubke, *J. Electrochem. Soc.* **132,** 1062 (1985).
7. W. N. Honeyman and K. H. Wilkinson, *J. Phys. D*: *Appl. Phys.* **4,** 1182 (1971).
8. K. Djessas, G. Massé, and M. Ibannaim, *J. Electrochem. Soc.* **147,** 1235 (2000).
9. Y. D. Tembhurkar, *Bull. Mater. Sci.* **20,** 1011 (1997).
10. S. P. Grindle, C. W. Smith, and S. D. Mittleman, *Appl. Phys. Lett.* **35,** 24 (1979).
11. R. Nomura, Y. Sekl, and H. Matsuda, *J. Mater. Chem.* **2,** 765 (1992).
12. S. Matsuda, Y. Kudo, T. Ushiki, H. Inoue, and K. Sato, *Jpn. J. Appl. Phys.* **31,** 999 (1992).
13. C. J. Carmalt, D. E. Morrison, and I. P. Parkin, *J. Mater. Chem.* **8,** 2209 (1998).
14. R. Hunger, D. Su, A. Krost, D. Ellmer, H. J. Lewerenz, and R. Scheer, *Thin Solid Films* **361–362,** 437 (2000).
15. J. Moon, T. Li, C. A. Randall, and J. H. Adair, *J. Mater. Res.* **12,** 189 (1997).
16. Q. Y. Lu, J. Q. Hu, K. B. Tang, Y. T. Qian, G. E. Zhou, and X. M. Liu, *Inorg. Chem.* **39,** 1606 (2000).
17. Y. Jiang, Y. Wu, X. Mo, W. C. Yu, Y. Xie, and Y. T. Qian, *Inorg. Chem.* **39,** 2964 (2000).
18. T. J. Trentler, K. M. Hickman, S. C. Goel, A. M. Viano, P. C. Gibbons, and W. E. Buhro, *Science* **270,** 1791 (1995).
19. R. S. Wanger, *in* "Whisker Technology." (A. P. Levitt, Ed.), Chapter 3, Wiley, New York, 1970.
20. N. L. Chen, "Handbook of Solvents," 2nd ed., 772, Chemical Industry Press, Beijing, 1994 (in Chinese).
21. JCPDS No. 27-159 for $CuInS_2$.
22. C. N. J. Wagner and E. N. Aqua, *Adv. X-Ray Anal.* **7,** 46 (1964).
23. C. D. Wagner, W. M. Riggs, L. E. Davis, J. F. Moulder, and G. E. Muilenberg, "Handbook of X-Ray Photoelectron Spectroscopy," Perkin-Elmer Corp., Eden Prairie, MN, 1978.
24. J. Llanos, A. Buljan, C. Mujica, and R. Ramirez, *J. Alloys Compd.* **234,** 40 (1996).
25. L. D. Partain, R. A. Schneider, L. F. Donaghey, and P. S. Mcleod, *J. Appl. Phys.* **57,** 5056 (1985).
26. R. Marquez and C. Rincon, *Phys. Status Solidi B* **191,** 115 (1995).
27. J. L. Shay and J. H. Wernick, "Ternary Chalcopyrite Semiconductors: Growth, Electronic Properties and Application," Pergamon, Oxford, 1975.
28. H. Weller, *Angew. Chem., Int. Ed. Engl.* **32,** 41 (1993).
29. M. Moffitt, L. McMahon, V. Pessel, and A. Eisenberg, *Chem. Mater.* **7,** 1185 (1995).